Scanning Tunneling Microscopy Studies of Ion-Bombarded Surfaces

By I. S. T. Tsong

Department of Physics and Astronomy,

Arizona State University, Tempe, AZ 85287, U.S.A.

and

P. Bedrossian

Lawrence Livermore National Laboratory

Box 808, L-350 Livermore, CA 94550, U.S.A.

Synopsis

The recent results in atom-resolved scanning tunneling microscopy studies of semiconductor crystalline surfaces of Si(111)-(7 × 7) and Si(100)-(2 × 1) bombarded by energetic ions are reviewed. Low-fluence bombardment introduces surface damage consisting of random vacancies varying in size from single atom to multiple atoms. Annealing the bombarded Si(100) surface between 600°C and 850°C causes the random defects to order into vacancy lines perpendicular to the dimer rows. High-fluence experiments at elevated temperatures show nucleation of vacancy islands on Si(100) and Si(111) surfaces. With increasing temperatures and ion doses, step retraction occurs on the Si(100) and Si(111) surfaces, indicative of layer-by-layer sputtering. In the Si(100)-(2 × 1) case, a striking metastable single type-A domain is formed on the surface. For comparison, experiments of low-fluence bombardment of Au(111), and high-fluence bombardment of Pt(111) and $Pt_{25}Ni_{75}$(111) surfaces are also briefly reviewed.

1 Introduction

A microscopic understanding of the interaction between energetic ions and solid surfaces became possible with the advent of the technique of scanning tunneling microscopy (STM). In this review, we will cover only those STM studies conducted in ultrahigh vacuum (UHV), i.e. where the base pressure of the experiment is at $\leq 1 \times 10^{-10}$ torr, because only at such vacuum are the starting surface and the tunneling conditions well-defined. There have been a number of STM studies

of ion-bombarded surfaces of graphite or related materials carried out under atmospheric conditions. Unfortunately, the well-known anomalies observed in STM images of graphite in air (Albrecht et al., 1988; Colton et al., 1988; Kuwabara et al., 1990; Heckl & Binnig, 1992) were not addressed in these studies. Neither has there been any attempt to conduct definitive studies on the possible changes in tunneling response associated with enhanced adsorption of oxygen and other contaminants on the bombarded surface exposed to air. In view of these deficiencies and uncertainties, ambient STM studies of ion-bombarded graphite will not be included here.

The STM experiments carried out thus far are divided into two categories: (a) the low-fluence approach, in which the effects of individual ion impacts are examined; and (b) the high-fluence approach, in which sputtering of the surface is treated as the inverse of crystal growth. The surfaces studied are by necessity single-crystalline in nature so that the STM can clearly discern the initial ordering and defect density (if any) prior to ion bombardment. The bombardment is carried out in situ, i.e. in the same UHV chamber in which STM studies are being conducted, to avoid contamination of the surface. This is to ensure that any change in topography, defect density and atomic order observed by the STM must be the consequence of ion bombardment.

In this review, we present a detailed discussion of STM results of ion bombardment of semiconductor surfaces, specifically Si(111) and Si(100) surfaces, obtained over the past two years by the authors. STM studies of ion-bombarded surfaces of metals and alloys, primarily carried out by the research groups of Stanford, Jülich and Vienna, are also briefly discussed.

2 Low-Fluence Experiments

Prior to bombardment, the Si(111) and Si(100) surfaces were cleaned by flashing to 1200°C for ~20 seconds to eliminate the native oxide layer. The pressure in the UHV chamber was kept at or below 2×10^{-9} torr when the sample was at 1200°C. After the heat treatment, the atom-resolved STM images of these two surfaces would show the familiar Si(111)-(7 × 7) and Si(100)-(2 × 1) reconstructions. It is important to keep the defect density of the clean surface as low as possible since certain defects appear as vacancies or adclusters which may be confused as effects due to ion bombardment. Transition metal contamination is a main contributor to these defects, and in order to avoid this, all parts in contact or in the vicinity of the silicon samples are constructed in either tantalum or molybdenum.

The Si(111)-(7 × 7) and Si(100)-(2 × 1) reconstructions are easily contaminated by oxygen and the contamination produces surface features, e.g. the appearance of

missing atoms, which could easily be mistaken as ion-bombardment damage (Liebsle et al., 1988; Avouris et al., 1991; Pelz & Koch, 1991; Kliese et al., 1992; Avouris & Cahill, 1992). To ensure that the STM was not imaging oxygen contamination, two tests were performed. The first was to leak the 99.9999% pure argon gas via the differentially pumped ion gun into the UHV chamber to a pressure higher than that used during ion bombardment for several minutes. It was confirmed by STM that the Si surfaces were not affected up to a pressure of 1×10^{-5} torr. The second test was to place the sample in the proximity of, but not actually in, the path of the Ar^+ ion beam for periods longer than that required to achieve a typical fluence. Once again STM images showed no sign of contamination of the silicon surfaces.

The clean Si(111) and Si(100) surfaces were bombarded by 3keV Ar^+ ions at normal incidence at fluences ranging from 7×10^{11} to 6×10^{12} ions cm^{-2}. 10^{12} ions cm^{-2} correspond to ~0.001 monolayer (ML) coverage. During bombardment, the pressure in the UHV chamber rose to 3×10^{-8} torr. Typical ion currents used were 5 - 10nA and the bombardment lasted a few seconds. The beam spot on the sample was 5mm in diameter.

The Si(111) and Si(100) surfaces before and after 3keV Ar^+ ion bombardment are shown in figs. 1 and 2 respectively. The defects created by ion bombardment are mainly in the form of missing atoms. These missing atoms tend to congregate to give the appearance of craters on the Si(111) and Si(100) surfaces. Usually in the vicinity of these craters, some bright spots are found. These are most likely adatoms or adclusters which originate from the sputtering process, perhaps due to atoms displaced from the nearby craters.

The appearance that the craters on the Si(111)-(7×7) surface are larger than those on the Si(100)-(2×1) surface can be easily understood from a consideration of the size of the 7×7 unit cell. The 7×7 has a unit cell edge of 27Å. The disappearance of four adjacent Si adatoms on the 7×7 surface would result in a pit of ~15Å × 15Å in area. Correspondingly, the disappearance of the same number of atoms on the 2×1 surface, e.g. two pairs of dimers on the same dimer row, would result in a pit area of only ~5Å × 5Å.

Over 200 STM images were taken by Zandvliet et al. (1992) on the ion- bombarded Si(111) and Si(100) surfaces and the results were remarkably consistent. From these images, we note that there are almost always more craters than the number of ion impacts. This means if we try to determine a sputtering yield from the number of missing atoms in the image, then the yield is always greater than 1 because each crater contains more than 1 missing atom. The sputtering yield determined by conventional methods (Zalm, 1988) for 3keV Ar^+ ions incident normally on Si is ~1. This suggests that at the very initial stages of sputtering, i.e. when the ion fluence is still insufficient to disturb the surface order, the sputtering yield may be higher than that measured at steady state, i.e. after the surface has been

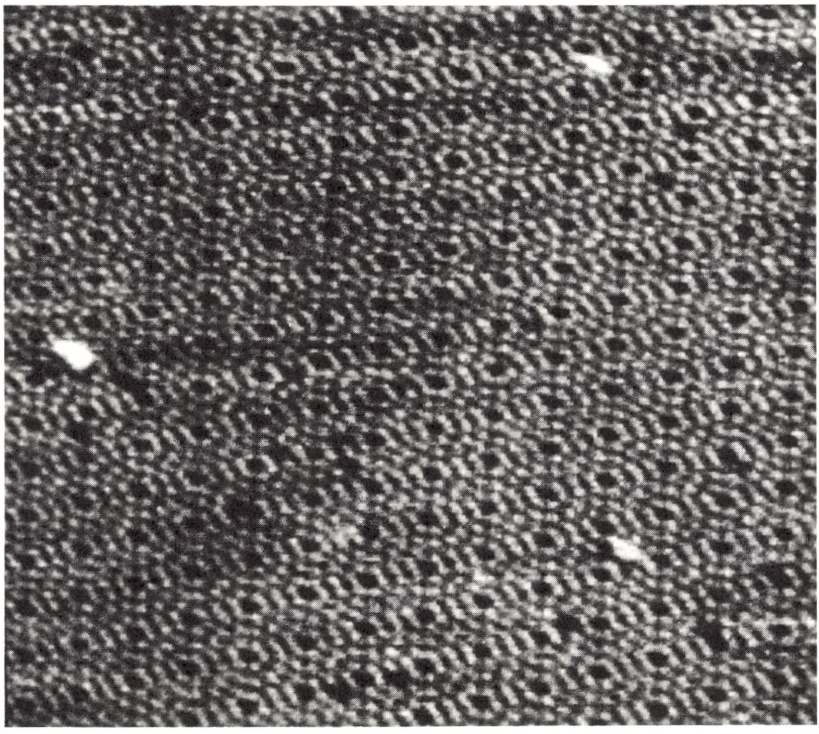

Figure 1a. STM image of Si(111)-(7 × 7) surface. Sample bias was 1.8V and tunnel current was 0.5nA. 40nm × 35nm scan of a clean surface showing the well-ordered 7× 7 reconstruction

impacted by high fluence and has become disordered. An observation of higher sputtering yield for an undamaged surface compared with a damaged surface has been reported for Ru(0001) by Burnett et al. (1989). On the other hand, the apparent large crater size observed in the images may not entirely be the result of sputtering. They could be the result of surface relaxation to relieve the strain produced by subsurface damage by the incoming ion as shown by Wilson et al. (1988). Classical molecular dynamics (MD) simulations by Feil et al. (1992) using a silicon microcrystallite consisting of 12 layers of 32 atoms each have reproduced some of the large craters observed on the Si(100) surface. Interestingly, however, in the same simulations, the number of atoms observed leaving the surface as sputtered atoms gives a sputtering yield of $\sim$1. Thus the MD simulations support the notion that the observed craters are not exclusively due to sputtering.

Zandvliet et al. (1992) showed that on annealing, the ion-bombarded Si(111)

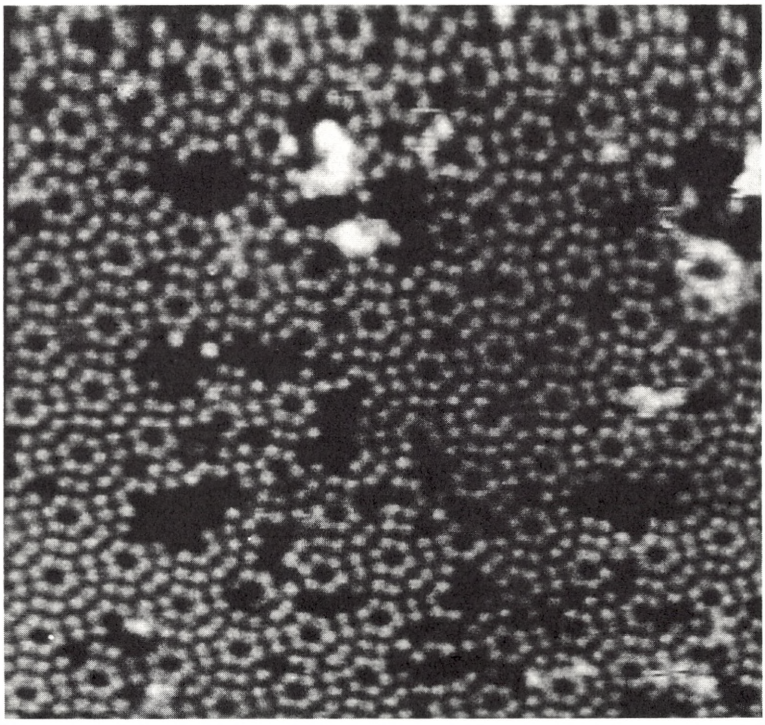

Figure 1b. Same as fig. 1a, but 25nm × 25nm scan of a surface bombarded by 3keV Ar^+ ions at a dose of $3 \times 10^{12}/cm^2$. A cratered appearance of the 7 × 7 structure is clearly visible.

and Si(100) surfaces produced contrasting results. The ion-bombarded defects or craters on the Si(111) surface disappeared totally when the surface was annealed at 750°C for 2 minutes and the 7 × 7 reconstruction was completely restored. The defects on the Si(100) surface, on the other hand, ordered into line defects perpendicular to the dimer rows as shown in fig. 3 upon annealing at temperatures between 600°C and 850°C for 2 minutes. When annealed at 950°C for 2 minutes, however, the line defects disappeared and the surface was restored to the original 2 × 1 state. No ordering of defects was observed at 500°C, indicating that the ordering threshold on the Si(100) surface was somewhere between 500°C and 600°C (Feil et al., 1992).

A likely mechanism for the ordering behavior on the Si(100) surface is that at elevated temperatures, the vacancies have preferential mobility along the dimer rows in addition to attractive interaction among themselves. When the vacancies

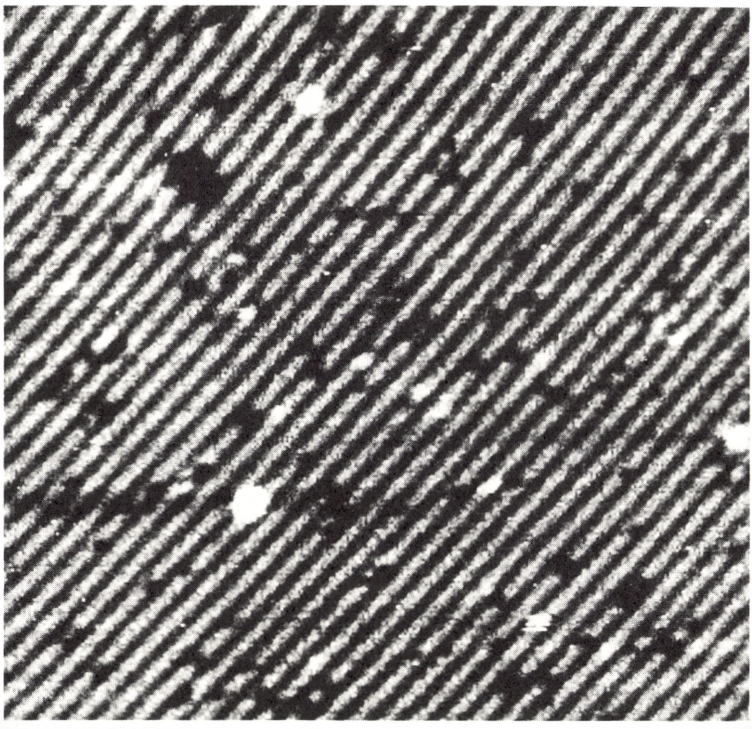

Figure 2a. STM image of Si(100)-(2 × 1) surface. Sample bias was -2.0V and tunnel current was 0.5nA. 20nm × 17nm scan of a clean surface showing the 2 × 1 reconstruction of dimer rows.

meet, they form the line defects observed in fig. 3. The question then arises on why the vacancies line up perpendicular to the dimer rows rather than parallel. Feil et al. (1992) performed quantum mechanical MD simulations using the ab initio real space tight-binding method of Sankey & Niklewski (1989) to seek an answer. In these simulations, the Si(100) surface was modeled by a five-layer slab repeated slab supercell, with the atoms in the bottom layer assigned huge masses and attached to hydrogen-like atoms to saturate their dangling bonds so that they were motionless and regarded as bulk atoms. Then a line of atoms (or dimers) was removed from the 2 × 1 surface and the atoms on the surface and in the exposed second layer were allowed to settle into their most favorable positions according to Newton's laws of motion. The total energies of the missing line perpendicular to the dimer rows and the missing line parallel to the dimer rows were then calculated and compared. Feil et al. (1992) found that the perpendicular case was favored by

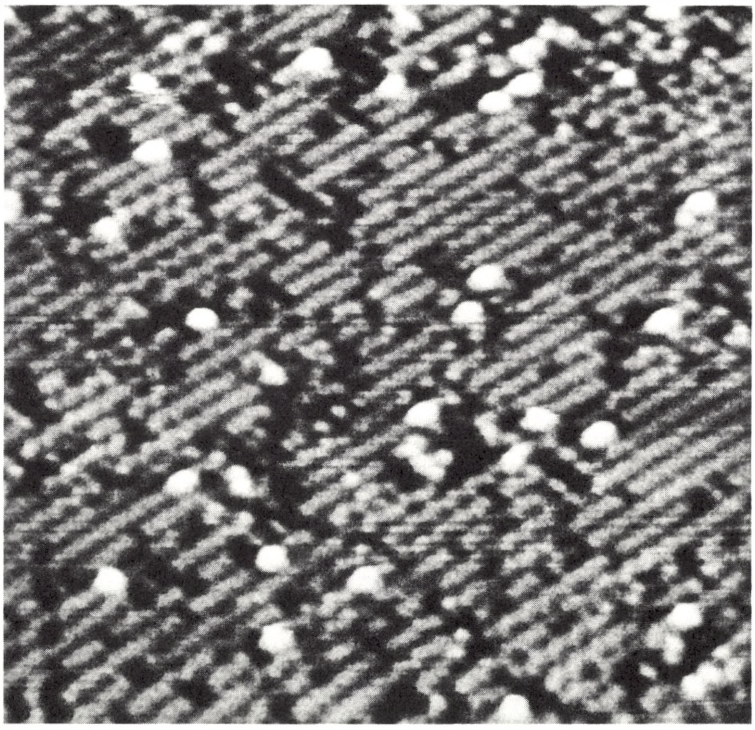

Figure 2b. Same as fig. 2a but 15nm × 22nm scan of a surface bombarded by 3keV Ar^+ ions at a dose of $3 \times 10^{12}/cm^2$. A pitted surface with missing dimers is observed.

having an energy lower by an amount of 0.011 eV/atom, in agreement with STM observations.

The depths of the sputtered craters on the Si(111) and Si(100) surfaces measured from the STM images are 2.1Å and 1.4Å respectively, suggesting that only the top layer surface atoms are missing or removed. This is not, however, conclusive evidence that sputtered atoms originate from the top layer because the observed craters or depressions may be a consequence of surface relaxation as discussed earlier. Due to the open structure of the silicon lattice, sputtering from second or deeper layers is conceivable as demonstrated by recent molecular-dynamics simulations by Smith et al. (1989) and experiments by Blumenthal et al. (1991). However, this may only be applicable to sputtering of an undamaged surface as high-fluence experiments in the next section provide convincing evidence of layer-by-layer sputtering.

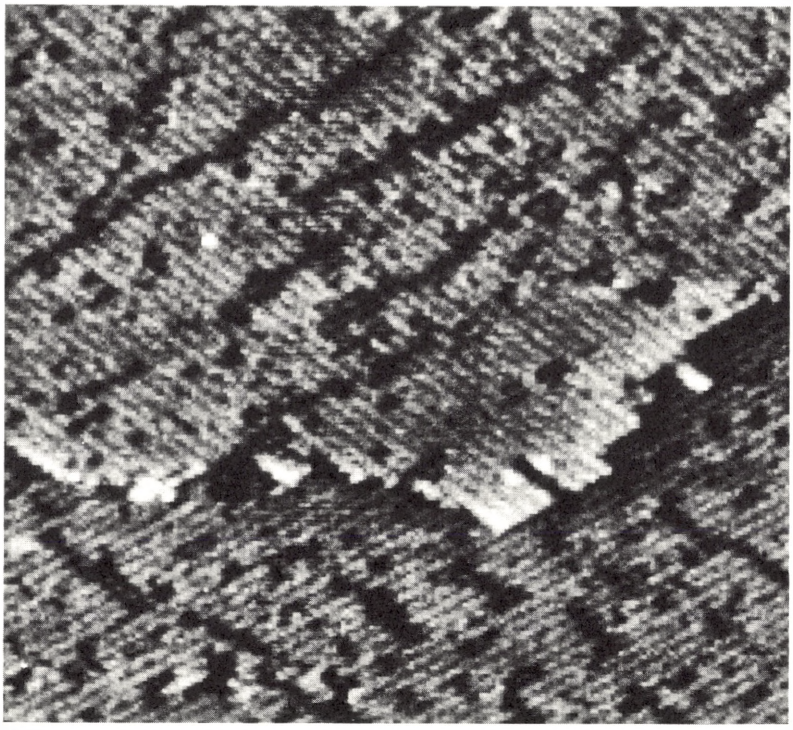

Figure 3. STM image of a bombarded Si(100)-(2 ×1) surface annealed at 750°C for 2 minutes. Scan area = 40nm × 40nm. Sample bias = -2.0V. Tunnel current = 0.5nA. The dimer vacancies ordered into lines perpendicular to the dimer rows on the type-B terrace (upper) and type-A terrace (lower) of the 2 ×1 surface.

STM studies of low-fluence Ne^+ ion bombardment at energies 3keV and 600eV on Au(111) surfaces under UHV conditions have been reported by Lang et al. (1991). They observed pits or craters on the Au(111) surface created by sputtering with a minimum diameter of 10Å, corresponding to approximately 10 atomic vacancies. Interestingly, the pit sizes showed an increasing trend with increasing ion fluence. The increase in pit size is probably due to the high mobility of vacancies on the Au surface even at room temperature, such that smaller pits tend to coalesce to form larger pits. This coalescent effect also explains why no pit sizes under 10Å were observed. Similar to the work of Zandvliet et al. (1992) on Si surfaces, the measured depth of the pits on Au(111) is 2.5Å, i.e. single atomic layer deep, suggesting that sputtering only removes the top-layer atoms.

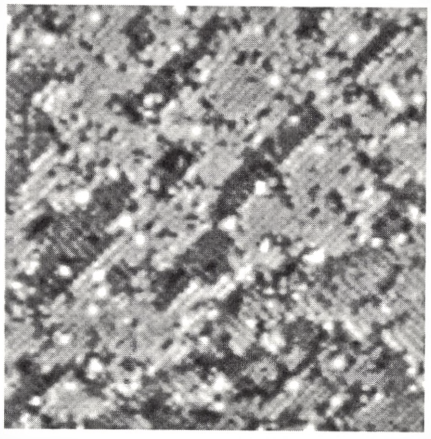

Figure 4. 360Å × 360Å STM image of Si(100)-2 ×1 following removal of ≈1/2 ML by 225eV Xe^+ sputtering with the substrate at 400°C. Anisotropic monolayer- deep depressions or vacancy islands (darker regions) are elongated parallel to the dimer rows of the top layer. The tip bias is +1.8V, so that occupied states are imaged.

3 High-Fluence Experiments

Bedrossian & Klitsner (1991, 1992) carried out STM studies of ion bombardment of Si(111)-(7 × 7) and Si(100)-(2 × 1) at high fluences ($>10^{15}$ ions/cm^2 and elevated temperatures. They showed that at sufficiently low ion energies, (≈200- 250eV) atomic-layer control of sputtering can be achieved. In an earlier study, Bedrossian et al. (1992) observed oscillations in reflection high-energy electron diffraction (RHEED) during glancing-angle, low-energy ion irradiation (200eV Xe^+) of Si(100)-(2 × 1) held at elevated temperatures, establishing that layer-by-layer removal from silicon can be accomplished under these conditions and implying that such a process may be described as the inverse of silicon homoepitaxial growth. Whereas the evolution of surface morphology during growth is mediated by mobile adatoms, which can either nucleate adatom islands or attach at step edges; layer-by-layer sputtering is found to be mediated by mobile surface vacancies which are created during sputtering and which can either nucleate monolayer-deep vacancy islands or annihilate at step edges. Monte Carlo simulations incorporating these processes have reproduced all of the RHEED observations (Chason et al., 1991).

STM has elucidated the kinetics and consequences of the signatures of layer-by-layer sputtering of silicon, vacancy island nucleation and step retraction. On Si(100), for example, one observes with increasing substrate temperature both a lower density and larger average size of vacancy islands for a given ion fluence,

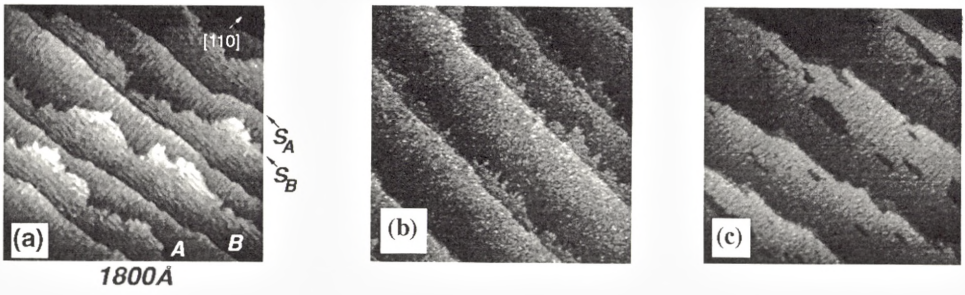

Figure 5. a) 1800Å x 1800Å image of 0.2°-offcut Si(100) showing predominantly straight S_A steps and wavy S_B steps on the 2 × 1 surface. b) 1800Å x 1800Å image following 225eV Xe^+ sputtering of ≈1/2 ML at 450°C, showing depletion of the type-B domain. c) 1800Å x 1800Å image following Xe^+ sputtering of ≈1 ML at 450°C, showing almost complete depletion of the type-B domain and nucleation of depressions or vacancy islands in the type-A domain.

consequences of increasing vacancy mobility with temperature. Fig. 4 shows an example of vacancy island formation on Si(100) following removal of ≈1/2 monolayer (ML) by 225eV Xe^+ ions incident at 75° from the surface normal, with the substrate held at 400°C. Because the dimer rows inside the vacancy islands are perpendicular to those in the outer layer, the vacancy islands are one monolayer deep (Chadi, 1987). The elongation of the depressions parallel to the dimer rows in the outer atomic layer indicates that mobile surface vacancies annihilate preferentially at the ends of dimer rows, just as the analogous elongation of growth islands along dimer rows has been ascribed to preferential sticking of adatoms at the ends of dimer rows (Hamers et al., 1989; Mo et al., 1989).

At still higher temperatures, a transition takes place from vacancy island nucleation to step retraction, analogous to step flow in epitaxial growth. For the case of Si growth on a substrate miscut towards the [110] direction, the preferential sticking of adatoms at the ends of dimer rows causes the S_B-step, which consists of the ends of dimer rows, to catch up with the S_A-step, which is parallel to a single dimer row, leading to a double-stepped, single-B-domain surface, on which all dimer rows lie perpendicular to the step edges (Sakamoto et al., 1987; Hoeven et al., 1987). Here, we use Chadi's notation (1987) for S_A and S_B steps. In the case of layer-by-layer sputtering, the preferential annihilation of vacancies at the ends of dimer rows leads to the retraction of the S_B-step relative to the S_A-step, as shown in fig. 5, resulting in a single-A-domain surface, a new surface phase of Si(100) which is not accessible by epitaxial growth. While the single-A-domain phase is not an equilibrium structure, it is stable at the temperature at which it was created. Its stability at typical growth temperatures therefore makes it a promising substrate

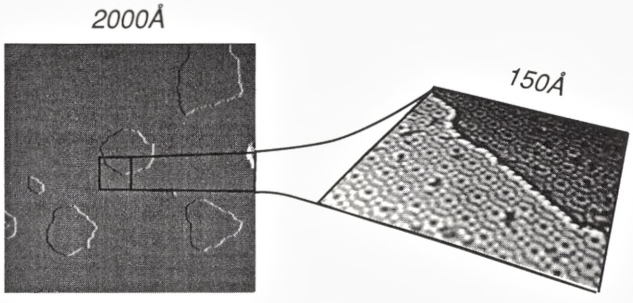

Figure 6. A 2000Å x 2000Å STM image and accompanying detail of a Si(111)-7 × 7 surface following 225eV Xe^+ bombardment at 580°C, showing monolayer- deep vacancy islands. The floor of the vacancy island in the enlarged image shows near-perfect 7 × 7 reconstruction. The tip bias is -1.8V, so unoccupied sample states are imaged.

for III/V-on-Si heteroepitaxy.

Layer-by-layer sputtering of Si(111) also proceeds via nucleation of vacancy islands, giving way to step retraction at elevated temperatures. In addition, one observes on this surface a second transition involving the surface periodicity itself. Layer-by-layer sputtering of Si(100) was found to preserve the 2 × 1 periodicity of that surface as low as 250°C. However, the Si(111) surface exhibits a transition from destruction to preservation of the 7 × 7 reconstruction with increasing substrate temperature (Bedrossian & Klitsner, 1991). Fig. 6 shows monolayer-deep vacancy islands formed after 225eV Xe^+ sputtering of Si(111)-7 × 7 at 580°C. As shown in the detail, the layer exposed by sputtering exhibits the 7 × 7 reconstruction.

In contrast, layer-by-layer sputtering at lower substrate temperatures can leave the exposed atomic layers with no long-range reconstruction. Fig. 7 shows the retraction of a step edge following an initial stage of sputtering of Si(111)-7×7 at 400°C. The material on the lower plane exposed by sputtering, immediately adjacent to the step edge, exhibits no long-range reconstruction. A sharp boundary separates this unreconstructed region from the fully reconstructed region. One may infer that the original step edge on the starting surface followed the path of this boundary. Purely physical sputtering can therefore not only induce the dereconstruction of the Si(111) surface, but can also cause selective dereconstruction adjacent to a step edge as in fig. 7.

STM studies of sputtering of Au(111) and Pt(111) surfaces by energetic ions at high fluence and at high temperatures have been conducted by the Jülich group (Michely et al., 1990; Michely & Comsa, 1991 a and b). In these experiments, sputtering acted essentially as a source of mobile monatomic vacancies, while lat-

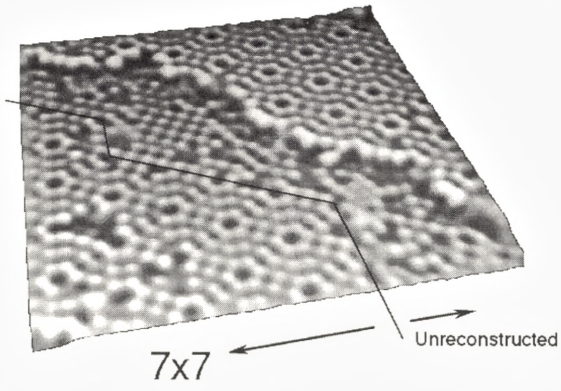

Figure 7. 150Å x 150Å image showing step retraction by 225eV Xe^+ sputtering of Si(111) at 400°C. The line separates the 7 ×7 region from newly exposed, unreconstructed material.

tice damaging effects were almost immediately annealed because of the elevated temperatures. Vacancy islands similar to those on silicon surfaces (Bedrossian & Klitsner, 1991 and 1992) were observed. Below 270°C, adatom islands were observed on Pt(111) in addition to vacancy islands. These adatom islands were formed by interstitials (of Frenkel pairs below the surface as a result of ion damage) diffusing to the surface layer forming adatoms which then coalesced to form islands. The adatom islands disappeared at or above 270°C leaving only vacancy islands. When the temperature was further increased to 350°C, the vacancy islands had an equilibrium hexagonal shape reflecting the symmetry of the (111) surface. As sputtering continued, STM images showed pits with depths of several monolayers. These pits consisted of hexagonal vacancy islands stacked one below another. The walls of each pit all had monolayer steps. The steps belonging to different layers generally did not touch and they maintained a constant pit slope. When sputtering was performed on Pt(111) at 440°C, the multi-layered pits were no longer observed. Instead, the STM images showed very large single-monolayer deep hexagonal vacancy islands. This surface morphology persisted even after the removal of 50 ML by sputtering and thus could be regarded as "steady-state" morphology attributable to layer-by-layer sputtering.

Schmid et al. (1992 a and b) have performed STM studies of preferential sputtering and recoil mixing of a $Pt_{25}Ni_{75}(111)$ alloy single crystal surface. Atom-resolved STM images of the sputtered surface annealed at 475°C clearly show dislocations which are attributed to sub-surface lattice mismatch dislocations reaching the surface. These mismatch dislocations are the result of preferential sputtering

leading to platinum enrichment in the upper layers, which in turn increases the lattice constant in those layers.

4 Conclusions

Scanning tunneling microscopy (STM) has provided a new way of studying the effects of ion bombardment on surfaces on an atomic scale. The proper experimental procedure involves surface cleaning and in situ bombardment under UHV conditions. At low ion fluences, the defects in the form of missing atoms, pits and craters created by individual ion impacts can be examined in detail. The shapes and sizes of the ion- bombarded defects and their ordering at high annealing temperatures observed in STM images can be compared with molecular dynamics simulations. High-fluence bombardment of surfaces at room temperature generally results in a highly disordered surface and undulating surface topography. However, when bombardment is carried at elevated temperatures, formation of vacancy islands due to mobile vacancies is observed. Further bombardment at high temperatures results in annihilation of vacancies at step edges of Si(100) and Si(111) and steady-state monolayer deep hexagonal vacancy islands on Pt(111), confirming a layer-by-layer sputtering process. Other interesting phenomena in sputtering such as preferential sputtering in an alloy has also been studied by STM. The last two years have seen the beginning of atom- resolved STM studies of sputtered surfaces. Many more experiments are certain to follow and new insights will continue to be gained.

Acknowledgements

ISTT thanks J. D. Dow, H. B. Elswijk, H. Feil, M. H. Tsai, E. J. van Loenen and H. J. W. Zandevliet for their contributions and Philips Research Laboratories for the award of a van Houten Fellowship for this work. PB's work was performed at Sandia National Laboratories in collaboration with E. Chason, J. E. Houston, T. Klitsner, S. T. Picraux, and J. Y. Tsao and was supported by BES, Office of Materials Science, Contract No. DE-AC04-76DP00789, and at Lawrence Livermore National Laboratory under the auspices of the U.S. Department of Energy under Contract W-7405-Eng-48.

References

Albrecht TR, Mizes HA, Nogami J, Park SI and Quate CF, 1988: Appl. Phys. Lett. **52**, 362
Avouris Ph and Cahill D, 1992: Ultramicroscopy **42-44**, 838
Avouris Ph, Lyo IW and Boszo F, 1991: J. Vac. Sci. Technol. B **9**, 424
Bedrossian and P Klitsner T, 1991: Phys. Rev. B **44**, 13783

Bedrossian P and Klitsner T, 1992: Phys. Rev. Lett. **68**, 646
Bedrossian P, Houston JE, Tsao JY, Chason E and Picraux ST, 1991: Phys. Rev. Lett. **67**, 124
Blumenthal R, Caffey KP, Furman E, Garrison BJ and Winograd N, 1989: Phys. Rev. B **44**, 12830
Burnett JW, Pellin MJ, Calaway WF, Gruen DM and Yates Jr JT, 1989: Phys. Rev. Lett. **63**, 562
Chadi DJ, 1987: Phys. Rev. Lett. **59**, 1691
Chason E, Bedrossian P, Horn K, Tsao J and Picraux ST, 1991: Appl. Phys. Lett. **59**, 3533
Colton RJ, Baker SM, Driscoll RJ, Youngquist MG, Baldeschwieler JD and Kaiser WJ, 1988: J. Vac. Sci. Technol. A **6**, 349
Feil H, Zandvliet HJW, Tsai MH, Dow JD and Tsong IST, 1992: Phys. Rev. Lett. **69**, 3076
Hamers RJ, Kohler U and Demuth JE, 1989: Ultramicroscopy **31**, 10
Heckl WM and Binnig G, 1992: Ultramicroscopy **42-44**, 1073
Hoeven AJ, Lenssinck JM, Dijkkamp D, van Loenen EJ and Dieleman J, 1989: Phys. Rev. Lett. **63**, 1830
Kliese R, Röttger B, Badt D and Neddermeyer H, 1992: Ultramicroscopy **42-44**, 824
Kuwabara M, Clarke DR and Smith DA, 1990: Appl. Phys. Lett. **56**, 2396
Lang CA, Quate CF and Nogami J, 1991: Appl. Phys. Lett. **59**, 1696
Liebsle FM, Samsavar A and Chiang TC, 1988: Phys. Rev. B **38**, 5780
Michely T and Comsa G, 1991a: Surf. Sci. **256**, 217
Michely T and Comsa G, 1991b: Phys. Rev. B **44**, 8411
Michely T, Besocke KH and Comsa G, 1990: Surf. Sci. Lett. **230**, L135
Mo YW, Swartzentruber BS, Kariotis R, Webb MB, and Lagally MG, 1989: Phys. Rev. Lett. **63**, 2393
Pelz JP and Koch RH, 1991: J. Vac. Sci. Technol. B **9**, 775
Sakamoto T, Kawamura T, Nago S, Hashiguchi G, Sakamoto K and Kuniyoshi K, 1987: J. Cryst. Growth **81**, 59
Sankey OF and Niklewski DJ, 1989: Phys. Rev. B **40**, 3979
Schmid M, Biedermann A, Stadler H, Slama C and Varga P, 1992a: Appl. Phys. A **55**, 468
Schmid M, Biedermann A, Stadler H and Varga P, 1992b: Phys. Rev. Lett. **69**, 925
Smith R, Harrison DE and Garrison BJ, 1989: Phys. Rev. B **40**, 93
Wilson IH, Zheng NJ, Knipping U and Tsong IST, 1988: Appl. Phys. Lett. **53**, 2039
Zalm PC, 1988: Surf. Interface Anal. **11**, 1
Zandvliet HJW, Elswijk HB, van Loenen EJ, and Tsong IST, 1992: Phys. Rev. B **46**, 7581